Vacuum 172 (2020) 109064

Contents lists available at ScienceDirect

Vacuum

journal homepage: http://www.elsevier.com/locate/vacuum

Micro-nano multilayer structure design and solid particle erosion resistance performance of CrAlNx/CrAlN coating

Di Wang [a,b], Songsheng Lin [b], Lingyun Liu [b], Hongzhi Yang [b,c], Jing Shi [a], Bailing Jiang [a], Kesong Zhou [a,b,c,*], Xiaofeng Zhang [b]

[a] School of Materials Science and Engineering, Xi'an University of Technology, Xi'an, 710048, China
[b] Guangdong Institute of New Materials, National Engineering Laboratory for Modern Materials Surface Engineering Technology, The Key Lab of Guangdong for Modern Surface Engineering Technology, Guangzhou, 510651, China
[c] State Key Laboratory of Powder Metallurgy, Central South University, Changsha, 410083, China

ARTICLE INFO

Keywords:
Cr-based coatings
Multilayer structure
Fracture toughness
Solid particle erosion

ABSTRACT

In this work, the CrAlNx/CrAlN micro-nano multi-layer structure coating was designed and prepared on TC11 titanium alloy by Arc Ion Plating (AIP). In addition, the monolayer CrN and CrAlN coatings was prepared for comparison. The effects of CrN and CrAlN monolayer, CrAlNx/CrAlN multilayer coatings on the micro-structure and phase composition were investigated by Scanning Electron Microscope (SEM), X-ray Diffraction (XRD), Transmission Electron Microscope (TEM), and Energy-dispersive X-ray micro-analysis (EDS). The mechanical properties of coatings, including nano-hardness, adhesion strength and fracture toughness were studied by means of nano-indentation, micro-scratch and indentation cracking (CSEM Instruments). It was found that the residual stress of CrN coating was −1.341 GPa, and that of CrAlN coating was −1.569 GPa, while that of CrAlNx/CrAlN multilayer coating was only −0.932 GPa significantly lower than that of CrN and CrAlN coatings. In addition, as the multilayer structure of CrAlNx/CrAlN (x is the atomic percentage, $x < 1$) is composed of nano-scale lamellar CrAlNx (L), thin columnar structure CrAlNx (C), and micro-nano-scale columnar structure CrAlN, the unique multilayer structure makes the highest fracture toughness (8.7 ± 0.5 MPa $m^{1/2}$). The minimum erosion rate was achieved for CrAlNx/CrAlN coatings under the condition of 1.265 ± 0.035 μm/g at 90° and 0.568 ± 0.022 μm/g at 30°, respectively. These results indicate that the CrAlNx/CrAlN multilayer coating has the excellent solid particle erosion resistance.

1. Introduction

During the low-altitude flights, take-offs and landings, dust and sand particles in the air can damage engine components under the action of high-speed airflow, especially the compressor blades at the front of the engine. Due to impact and wear, the shape and structural integrity of the compressor blades will be destroyed, which results in the degradation of the engine performance and service life, and serious effect on the work efficiency and safety [1–5].

The common method of blade resistance to solid particles erosion is to deposit an anti-erosion coating (mainly TiN-based [6–8]) on the surface of the compressor blade by physical vapor deposition. In order to improve the air pressure efficiency of the compressor, the compressor blades are usually curved, and the solid particles in the air will attack the erosion resistant coating deposited on the compressor blades from different angles. Hard coating has high hardness and good wear resistance, which can solve the micro-cutting problem under the small angle of attack. However, due to the lack of toughness of the hard coating, the wear resistance of the hard coating to solid particles is often insufficient under the condition of high angle of attack [9].

At present, many researchers focused on the toughening of anti-erosion coatings. Among them, the design of coating structure is the key point. The coating with multilayer structure has the ability of dispersing energy and transferring interlayer cracks, which can improve the toughness of the coating. In addition, different set of soft/hard multilayers like Ti/TiN [10], TiAl/TiAlN [11] and Ti/TiSiCN [12] were reported. Most of these reports claim that the multilayer coatings have better erosion resistance than single phase nitride coating. Even a unique multi-layer Ti–N coating system were developed by the Praxic Surface Technology Co. Ltd [13]. for the erosion protection of

* Corresponding author. School of Materials Science and Engineering, Xi'an University of Technology, Xi'an, 710048, China.
E-mail addresses: 343585114@qq.com (D. Wang), kszhou2004@163.com (K. Zhou).

https://doi.org/10.1016/j.vacuum.2019.109064
Received 26 October 2019; Received in revised form 7 November 2019; Accepted 7 November 2019
Available online 12 November 2019
0042-207X/

compressor blades. However, in the above report, the erosion resistance of the coating under high angle of attack is significantly worse than that of the coating under small angle of attack, so the improvement of toughness is still the main target of the erosion resistant coating. It is reported [14,15] that, the multilayer combination of Cr and CrN layers provides the coating with high adhesion strength, wear resistance, erosion resistance and high fracture toughness. Furthermore, the elastic modulus, nano hardness and wear resistance of CrN coatings can be improved by adding a third element such as Al [16].

Based on the Cr-based coating, a micro-nano-layered structure was designed to reduce the residual stress and improve the toughness, and three kinds of Cr-based coatings (CrN, CrAlN, CrAlNx/CrAlN) were deposited on the titanium alloy. The microstructure, mechanical properties and solid particle erosion resistance of the three coatings were systematically studied. Finally, the erosion damage mechanism of CrAlNx/CrAlN multilayer coating was discussed.

2. Experimental

2.1. Design of micro-nano multilayer structure

There are obvious micro-particles exist in the multi-layer coatings which prepared by Arc Ion Plating (AIP) technology, this result has been confirmed in the literature [17]. And some even run through the whole coating, which has a great negative impact on its mechanical properties [9]. It has been found that the multi-layer structure can block the growth of the columnar coating, but the connection between the layers were different columnar structures, and some micro-channels still exist in the interface between the layers which facilitate the propagation of cracks. Therefore, in the process of preparing the multi-layer coating by arc ion plating technology, grain refinement and blocking inter-layer micro--channels are the key factors to improve the performance of the coating.

The multi-layer coating (Fig. 1) studied in this paper constitutes a plurality of cycles, in which there is a cycle consisting of a CrAlNx (x is the atomic percentage, $x < 1$) metal-rich phase layer and a CrAlN ceramic phase layer. The multi-layer crack arrest principle and high-energy ion bombardment process design have realized the fragmentation (flattening) of micro-particles and deposited a multi-layer structure coating which combined a lamellar layer and a columnar one. In one cycle, the gradient of the bombardment gradient of ions during deposition forms an excessive gradient of morphology and composition. The lamellar structure completely eliminates the vertical micro-channel between the layers, thereby more effectively hindering the propagation of the crack. The specific deposition preparation process of the coating is as described in Section 2.2.

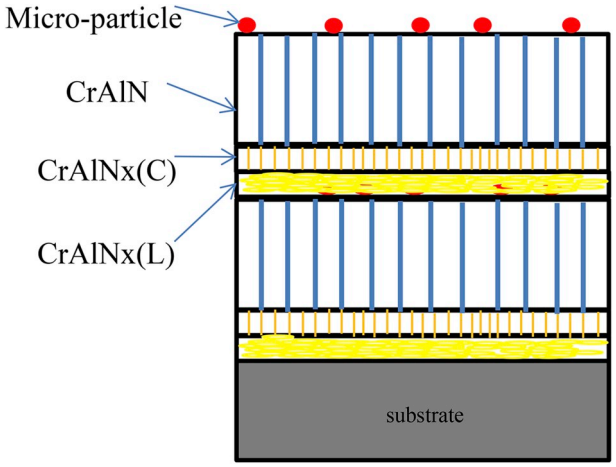

Fig. 1. The multi-layer coating schematic diagram.

2.2. Coating preparation

The Cr-based coatings were deposited by an industrial AIP system (AS700DTX, see the schematic of Fig. 2). There are a total of 8 circular targets in the chamber, including 4 targets of chromium (99.9%, mass fraction) and 4 composite targets of $Cr_{0.5}Al_{0.5}$ alloy (99.9%, mass fraction, Cr and Al content of 50 at %, respectively). The substrate materials were silicon and TC11 titanium alloy (5.8%–7.0% Al, 2.8%–3.8% Mo, 0.8%–2.0% Zr, 0.2%–0.35% Si). The phase composition were characterized by silicon-based coating and its micro-morphology was observed. The adhesion, hardness, fracture toughness and solid particle erosion resistance of the coatings on TC11 titanium alloy substrates were tested. The deposition parameters of CrN, CrAlN and CrAlNx/CrAlN coatings are listed in Table 1. The preparation and application of the multilayer coating are described in detail. The multi-layer coating schematic diagram is shown in Fig. 1.Each cycle contains three steps:

(1) Deposition parameters: current 110 A, pressure 0.5 Pa. Under conditions of high current and low pressure, the bombardment energy of deposited particles is the highest, and the coating is prone to form lamellar structure easily;
(2) Deposition parameters: current 90 A, pressure 1.5 Pa. A thin columnar metal-rich stress absorption layer CrAl (C) was formed;
(3) Deposition parameters: current 90 A, pressure 4.0 Pa. Under the condition of low current and high pressure, CrAlN coating can be obtained by reducing the droplet spatter and increasing particle collisions in the vacuum cavity.

2.3. Structural characterization

The surface and cross-section morphology of Cr-based coatings were characterized by Scanning Electron Microscope (SEM, Nova Nano SEM 430). The crystal structure of the coating was revealed by Grazing Incidence Small Angle Scattering X-ray Diffraction (GISAXS-XRD, Philips X'Pert3 Powder) from 10° to 90° at an increment of 0.02°. Transmission Electron Microscope (TEM) characterization and STEM-EDS analysis were performed by a FEITecnai G2F30 equipped with a high-angle annular dark-field detector (HAADF) and an Energy-dispersive

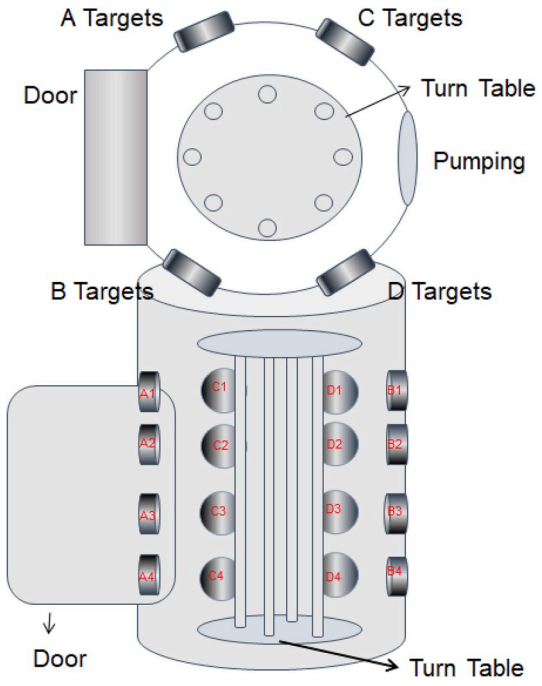

Fig. 2. Schematic diagram of industrial Arc Ion Plating equipment (AS700DTX).

Table 1
The deposition parameters of CrN, CrAlN and CrAlNx/CrAlN coatings.

interlayer	CrN	CrAlN	CrAlNx/CrAlN		
			CrAlNx		CrAlN
Current/A	90	90	110	90	90
N_2 pressure/Pa	4	4	0.5	1.5	4
Time/min	120	120	3	2	10
cycle			8		

X-ray Micro-analysis (EDS) system.

2.4. Mechanical characterization

The adhesion strength was tested by HH-3000 scratch tester. The maximum load of 100 N, the loading speed of 100 N/min and the scratch speed of 5 mm/min were applied in the course of the scratch measurement. The Nano Hardness (H) and Elastic modulus (E) were determined by a Nano Test 600 nano-mechanical system (Micro-Materials Ltd, UK). The indentation depth was 200 nm, less than 1/10 of the coating thickness to reduce the influence of the substrate on hardness. An average of 25 repeated indentations were taken from each specimen. The curvature of the substrate before and after the coating was measured by laser scanning, and then the residual stress of the coating was calculated according to Stoney formula [18].

$$\sigma = \frac{E_s}{6(1-\nu_s)} \frac{h_s^2}{h_c} \left(\frac{1}{R_2} - \frac{1}{R_1}\right) \quad (1)$$

where, Es: the modulus of elasticity of the substrate material, υs: the Poisson's ratio of the substrate material, hs: the thickness of the substrate, hc: the thickness of the coating.

Fracture toughness was measured by indentation cracking method. At a load of 300 mN, indents were made on the coatings with a cube corner indenter. These indents were observed in SEM to find the radial crack length 'C' (from the crack centre to the edge). Lawn et al. [19] showed the relationship between the length of radial crack, C and fracture toughness 'KC' as shown in the following equation:

$$K_c = 0.036 \times \left(\frac{E}{H}\right)^{\frac{1}{2}} \left(\frac{P}{c^{\frac{3}{2}}}\right) \quad (2)$$

where, E: modulus of elasticity, H: hardness, P: peak indentation load, c: radial crack length.

2.5. Solid particle erosion experiment

The solid particle erosion experiments were conducted on the self-designed AS600 sandblasting test machine as per ASTM G76-13standard [20], and the schematic diagram and detailed description of the erosion test machine device were provided in Ref. [9]. Based on the preliminary experiment, the particle velocity was controlled to be 30 ± 2 m/s, and the working distance between specimen and the outlet of nozzle was 10 mm. The impingement angle was set as 30° and 90°, respectively. The depth of erosion pits was measured by Bruker DEKTAX profile-meter. The solid abrasive particles of the erosion test were Al_2O_3 angular particles with an average size of 80 μm. The SEM micrograph and EDX elemental contents of the Al_2O_3 particles is shown in Fig. 3.

3. Results and discussion

3.1. Microstructure and phase composition

Fig. 4 shows the SEM surface and cross-section morphology of CrN, CrAlN monolayer and CrAlNx/CrAlN multilayer coatings. It can be seen that all the coatings exhibit analogous morphology with some macro-particles and pinholes on the surface. Among them, the CrN coating (Fig. 4(a)) has a flat surface with the least number of micro-particles, while the CrAlN coating (Fig. 4(c)) and CrAlNx/CrAlN coating (Fig. 4 (e)) have a large number of micro-particles. And the chemical composition of the three samples is shown in Table 2. The surface of the coating has a small amount of oxygen. It is mainly unavoidable that oxygen in the air is adsorbed on the surface of the coating.

It can be seen from the cross-section morphologies that these three

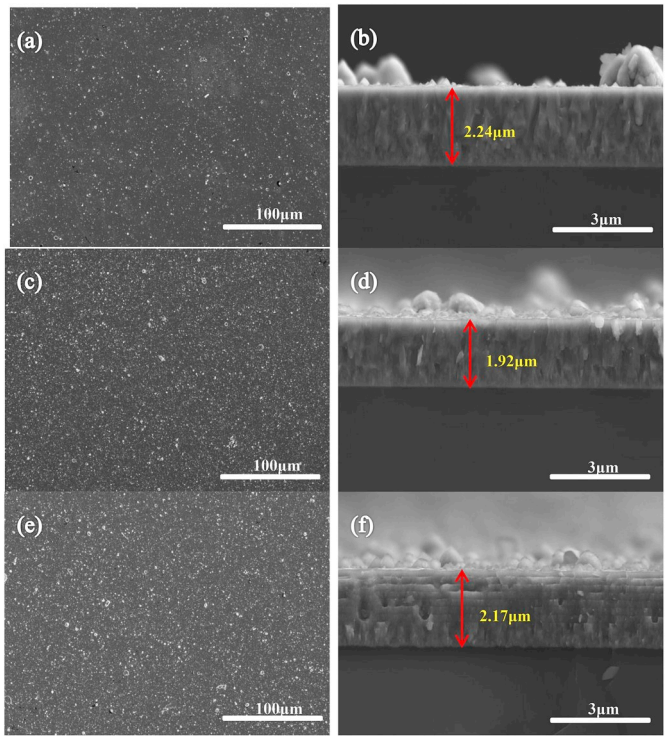

Fig. 4. Surface and cross-section morphology of Cr-based coatings (a) (b) CrN, (c)(d) CrAlN, (e)(f) CrAlNx/CrAlN.

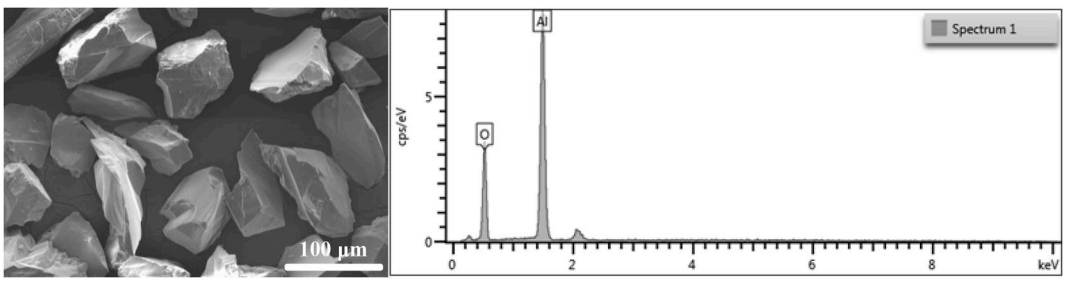

Fig. 3. Surface morphology and elemental contents of alumina (Al_2O_3) angular particles.

Table 2
The EDS spectrum results of Cr-based coatings in Fig. 4

	Cr %	Al %	N%	O%
CrN	77.87	/	20.52	1.61
CrAlN	25.40	23.07	50.16	1.37
CrAlNx/CrAlN	37.72	27.83	33.22	1.23

coatings are columnar structures, and the columnar structure of multilayer CrAlNx/CrAlN coating is significantly more thiner and closely arranged than the that of monolayer CrN and CrAlN coatings. The thickness of the coatings can be measured, The monolayer CrN coating (Fig. 4(b)) has a thickness of 2.24 μm, the monolayer CrAlN coating (Fig. 4(d)) is 1.92 μm and the thickness of the multilayer CrAlNx/CrAlN coating is 2.17 μm. The deposition rates of the coatings can be calculated by the thickness, as 1.12 μm/h, 0.96 μm/h and 1.085 μm/h, respectively.

Fig. 5 gives the XRD patterns of CrN, CrAlN and CrAlNx/CrAlN coatings. It shows that the crystal structure of Cr-based coatings are predominantly cubic crystal of CrN. The diffraction peaks of the coatings are mainly (111), (200) and (220). In addition, due to the incorporation of Al into the CrA1N and CrA1Nx/CrA1N coatings, the positions of these diffraction peaks gradually shift towards the higher diffraction angles (Fig. 5). The above results indicate that the lattice structure of the CrAlN coatings formed a solid solution, and Cr atoms were substituted by Al atoms since the covalent radius of Al (0.121 nm) is smaller than that of Cr (0.139 nm). This also leads to the deviation of the diffraction peak of the coating [21].

A more detailed picture of the microstructure and phase composition of the CrAl/CrAlN coating are provided by the cross-sectional TEM images and SAED pattern, as shown in Fig. 5. It can be seen that the modulation layer of the multi-layer coating is straight, and the interface is clear. The multilayer structure is divided into three layers, including a 150 nm columnar CrAlN layer, a 25 nm extremely dense columnar CrAlNx(C) layer, and a 25 nm lamellar CrAlNx(L) layer. The structure of the whole coating is constant. The thickness ratio of CrAlNx(C), the CrAlNx (L) and the CrAlN layer is about 1:1:6, which has regularity. It is found that the CrAlNx/CrAlN coating is a nano-poly-crystalline structure from the SAED pattern. And the coating is mainly composed of CrN main phases (111), (200) and (220). This result is consistent with the XRD results.

Fig. 6(a) shows a high-multiple cross-sectional TEM images. It can be seen that since a column may be consisted of several grains or subgrains, the grain size is usually smaller than the column width. The width of the CrAlN column is about 20 nm, and the width of the column

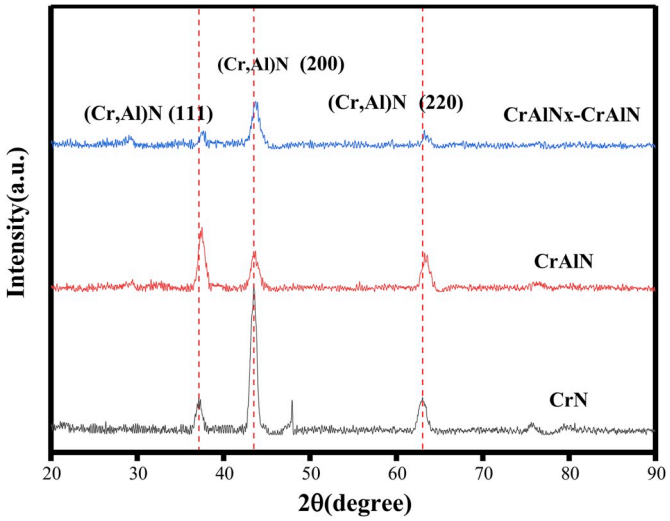

Fig. 5. XRD patterns of Cr-based coatings.

of the CrAlNx(C) layer grown by the columnar structure is merely 3 nm. The distribution of the grain size is homogeneous. This fine grain size is related to the ion bombardment during the coating growth, which produces many radiation defects. The defect density is sufficiently large to disrupt the columnar structure and cause periodic nucleation of new columns, thus inhibiting large grains [22]. If the ion bombardment energy is strong enough to cause the grain to slip along the dense surface, a lamellar morphology (CrAlNx(L)) will be generated, as shown in Fig. 6 (a).

Fig. 7(b), (c) and (d) are High Resolution Transmission Electron Microscopy (HRTEM) images of region 1(CrAlN layer), region 2(CrAlNx (C) layer) and region 3(CrAlNx(L) layer) in Fig. 7(a). It can be seen that the CrAlN layer is a single cubic CrN phase layer. And in the CrAlNx(C and L), a high density of defects (dislocations) within the individual grains was evident. The $Al_{13}Cr_2$ mono-clinic crystals were detected in CrAl (C and L) with representative crystal faces of (530) and (−132), and the lattice spacing was 0.21 nm and 0.24 nm, respectively. According to literature [23], the $Al_{13}Cr_2$ phase is the lowest phase of the Gibbs free energy in the AlCr alloy phase, so it is the easiest phase to form. At the same time, cubic AlN ceramic phases were found in the CrAlNx layer region and grew along the (110) densely packed surface. Therefore, the metal-rich layer CrAlNx(L and C) is a large amount of nano-$Al_{13}Cr_2$ crystal phase wrapped with a small amount of nano-AlN ceramic crystal phase. The EDS spectrum results of these three regions are shown in Table 3. It is found that there is less nitrogen in the regions 2 and 3, which means the design of the metal-rich phase layer of the coating is realized. In the region 3 (CrAlNx(L)), the Cr content was significantly decreased and the Al content increased. Interestingly, the alloy target of Cr50Al50 was used in this work. Therefore, the changes of Cr and Al contents in the coating are mainly due to the reverse sputtering effect of the coating deposition process. The difference in sputtering yields (Cr: 0.87/300eV, Al: 0.65/300eV) of the two elements leads to the difference in the final content [24].

3.2. Mechanical properties

Table 4 shows the mechanical properties of the Cr-based coatings, including nano-hardness, elastic modulus, adhesion strength, fracture toughness and residual stress. It can be found that the hardness of CrN (21.4 ± 0.5 GPa) is the lowest, while the hardness and elastic modulus of CrAlN and CrAlNx/CrAlN coatings have little difference. Due to the minimum residual stress (−0.932 GPa), the CrAlNx/CrAlN coating has the highest adhesion strength (46.2 N) and fracture toughness (8.7 ± 0.5 MPa $m^{1/2}$) is. Interestingly, the adhesion strength of the CrN coating is higher than that of CrAlN coating, but the fracture toughness and residual stress are both lower. Hardness and toughness are generally considered to be contradictory, but CrN has the lowest hardness and toughness. In order to explore this phenomenon, it can be seen from the comparison of indentation morphology that the indentation crack of CrN is significantly longer (Fig. 8). This is mainly due to the small number of micro-particles on the surface, which has little effect on the transverse propagation of the indentation crack. However, there are many micro-particles in the CrAlN and CrAlNx/CrAlN coatings. During the propagation of indentation cracks, the particles hinder the propagation distance of transverse crack and increase the toughness value. These micro-particles can be understood as the ductile phase of inlays with in the coating. The studies [25] showed that in coatings with ductile phases, when the crack approaches the interface, it can be redirected along the interface and deflected at the interface. When the release rate of strain energy changes significantly, the crack can stop. However, it can also lead to premature stratification. The results show that the existence of micro-particles in the coating plays a certain role in hindering the transverse propagation of cracks to some extent (see).

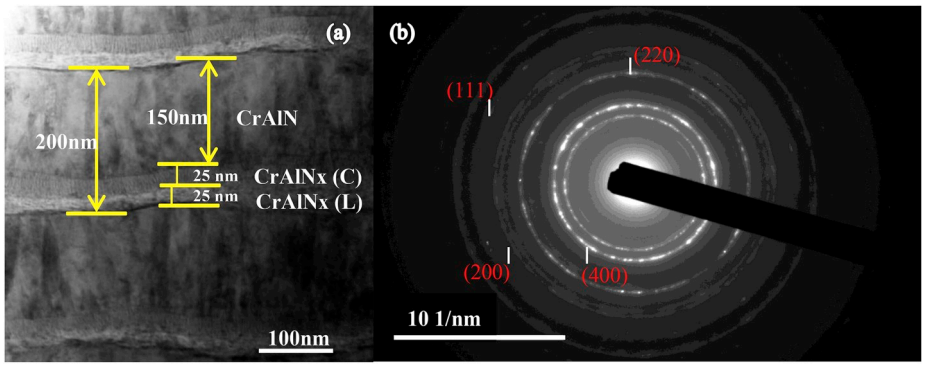

Fig. 6. Cross-sectional TEM images and Selected Area Electron Diffraction (SAED) pattern of the CrAlNx/CrAlN coating.

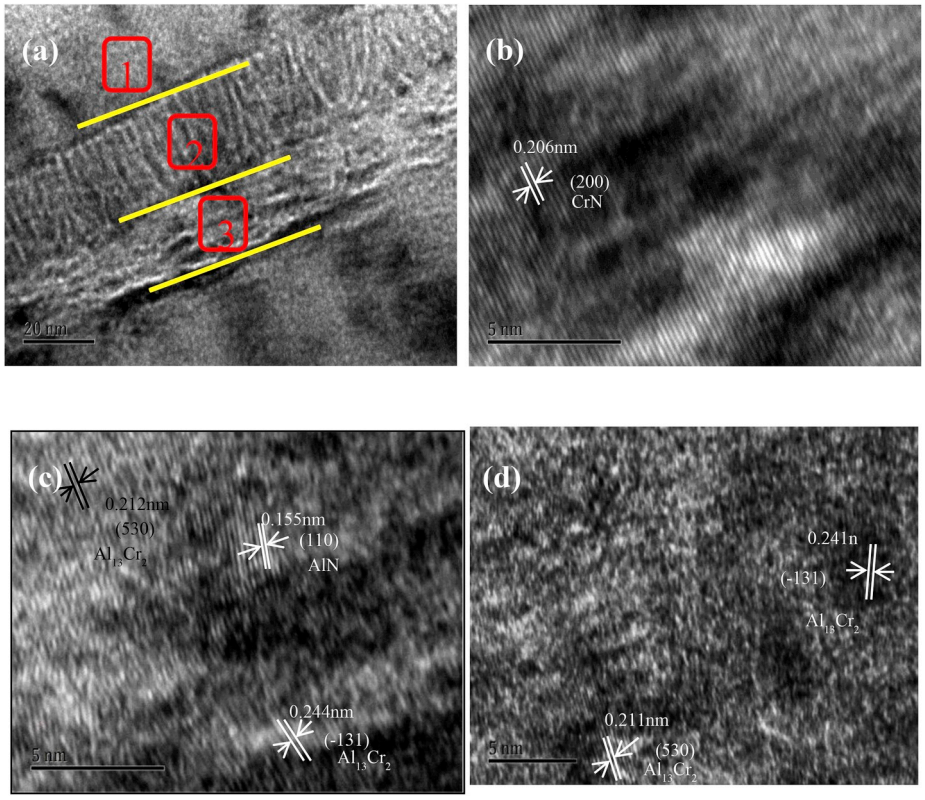

Fig. 7. CrAlNx/CrAlN coating (a) high-fold Cross-sectional TEM image; (b), (c), (d) high resolution transmission electron microscopy (HRTEM) images.

Table 3
The EDS spectrum results for three regions in Fig. 7(a).

	Cr %	Al %	N%
1	28.43	27.85	43.72
2	33.46	34.94	31.61
3	20.31	52.41	27.28

Table 4
Mechanical properties of the Cr-based coatings.

	H/GPa	E/GPa	Adhesion strength/N	Fracture toughness/ MPa·m$^{1/2}$	Residual stress/GPa
CrN	21.4 ± 0.5	280 ± 8	42	5.1 ± 0.2	−1.341
CrAlN	24.9 ± 0.3	331 ± 10	37.4	5.6 ± 0.3	−1.569
CrAlNx/ CrAlN	24.7 ± 0.6	324 ± 11	46.2	8.7 ± 0.5	−0.932

3.3. Solid particle erosion

Fig. 9 shows the erosion rates of the Cr-based coatings at 30° and 90° impact angles. The erosion rates are calculated based on the erosion depth per gram of sand in erosion test. As can be seen from Fig. 8, the erosion rate of the Cr-based coatings exhibited lower at 30° angle and higher at 90° angle. At 30°, the erosion rate of CrAlN coating was the lowest (0.474 ± 0.036 μm/g), followed by that of CrAlNx/CrAlN (0.568 ± 0.022 μm/g), and that of CrN was the highest (0.672 ± 0.034 μm/g). At 90°, the erosion rate of CrAlNx/CrAlN coating was the lowest (1.265 ± 0.035 μm/g), while that of CrAlN coating was the highest (1.643 ± 0.028 μm/g). It was also found that the erosion rate of CrN coatings with the worst toughness was 1.532 ± 0.031 μm/g, which was lower than that of CrAlN coatings. This indicates that the fracture toughness is not the decisive factor of erosion resistance at the high erosion angle. The presence of micro-particles in the coating only hinder the horizontal crack propagation, but provides a channel for crack propagation and promote it in the vertical direction. The

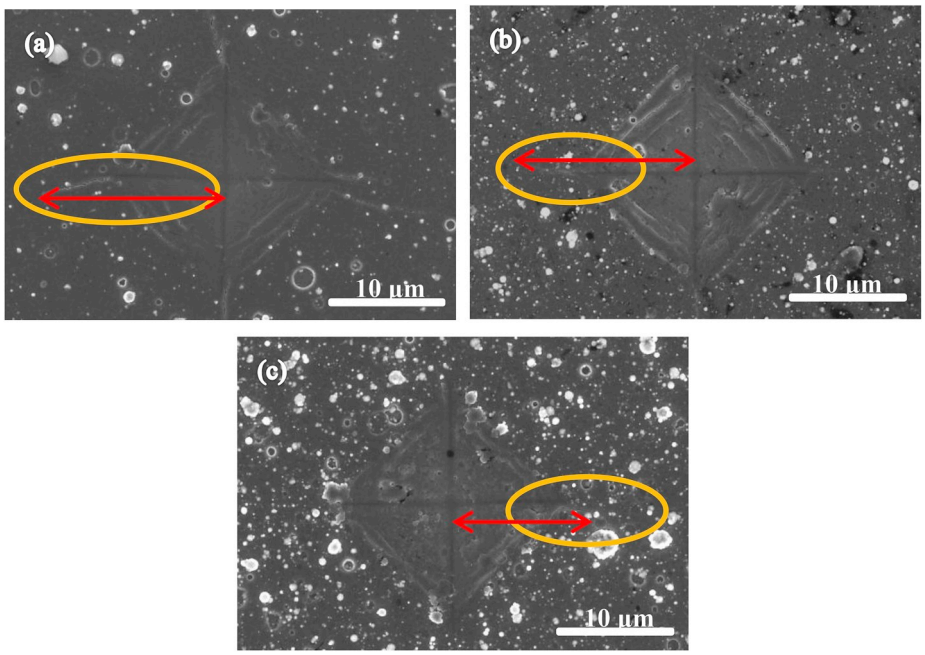

Fig. 8. Indentation morphology of Cr-based coatings(a) CrN, (b) CrAlN, (c) CrAlNx/CrAlN.

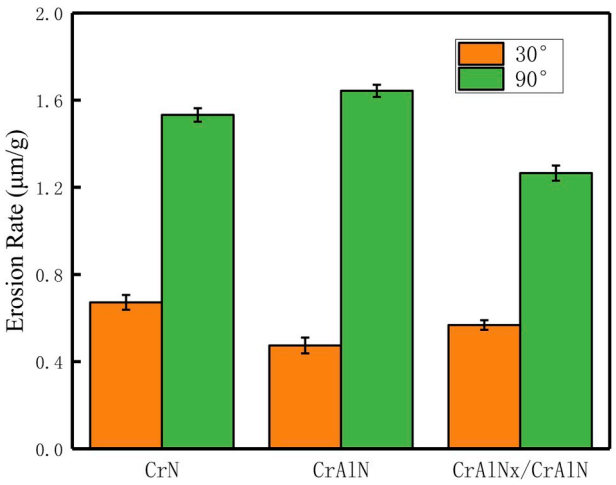

Fig. 9. Erosion rates of Cr-based coatings at 30° and 90° impact angles.

multilayer structure of CrAlNx/CrAlN coating has a variety of interlayer interfaces and grain distribution, which can effectively inhibit the horizontal and vertical propagation of cracks. From the above results, the average erosion rates of Cr-based coatings can be calculated at 30° and 90° erosion, CrN 1.102 ± 0.033 μm/g, CrAlN 1.059 ± 0.032 μm/g, and CrAlNx/CrAlN 0.916 ± 0.029 μm/g. The results show that the multilayer CrAlNx/CrAlN coating with high hardness and good toughness achieve excellent erosion resistance.

Many researchers have discussed the erosion failure process of monolayer nitride coatings [3,6,26]. Therefore, the erosion mechanism of multilayer coatings is analyzed in detail. Fig. 10 presents the morphology of the CrAlNx/CrAlN coating after 30° and 90° solid particle erosion experiment. Fig. 9 (a), (b) are the macroscopic views of the erosion scar regions of 30° and 90°, respectively, which are divided into three parts from the inside to outside: I. Severe washed area (partial coating peeling off); II. Edge washing area (elastic loading deformation); III. Unwashed area (intact coating). Therefore, in the process of erosion, it is easy to understand that the coating goes through the following three stages: 1. Intact coating; 2. A small amount of coating deformation and damage caused by sandblasting; 3. A large number of coatings falls off, forming erosion pit.

The edge and center of the erosion scar were observed to further investigate the erosion process of the CrAlNx/CrAlN coating. Fig. 10 (c) and (e) show the edge and central area after sanding at 30°, respectively. It can be seen that the coating in the edge region has only a small amount of damage, while the coating in the central region is obviously incomplete, and the surface cracks and debris increase significantly. Fig. 10 (d) and (f) show the edge and central area after 90° sanding, respectively. Irregular pits (or indentations) can be easily observed in the edge region. This is probably due to the removal of a surface chip on the edge of indentations caused by the impact of particles. The central area is the shape of a large amount of sand, the coating is severely damaged. There are many layers of spalling and some sand indentation.

In order to discuss the erosion failure mechanism of the CrAlNx/CrAlN coating, the central regions of 30° and 90° are magnified, as shown in Fig. 9 (e) and (f). At 30° (Fig. 9 (e)), when the impacted particles strike the surface of the coating, the movement of impacted particles is decomposed into horizontal and vertical ones [27]. The horizontal movement of impacted particles plays a leading role in dominating the material loss on cutting or plowing material surface. The process is mainly related to plastic deformation. The vertical splitting motion of the impacted particles causes radial cracking of the coating surface, and the coating material is removed by the combination of plastic cutting and radial cracking. The breakage of Al_2O_3 particles on the erosion scar indicates that the coating is plastic, and also indicates the secondary erosion caused by particle breakage. The broken process utilizes some portion of the kinetic energy of the incident particles. At 90° (Fig. 9 (f)), the mechanism of CrAlNx/CrAlN coating removal can be understood as: the coating surface is continuously affected by angular erodent particles. Micro-cracks may be generated and extended laterally underneath the surface of samples. Once these cracks are connected with each other during the process of successive erosion, local areas of the materials will be delaminated. Furthermore, pits left by the shedding of micro-particles can also be observed, indicating that stress concentration points are easy to form here, thereby accelerating the propagation of cracks, which have certain negative effects under both conditions of 30° and 90° erosion.

According to the microstructure of CrAlNx/CrAlN coating (Fig. 5), it

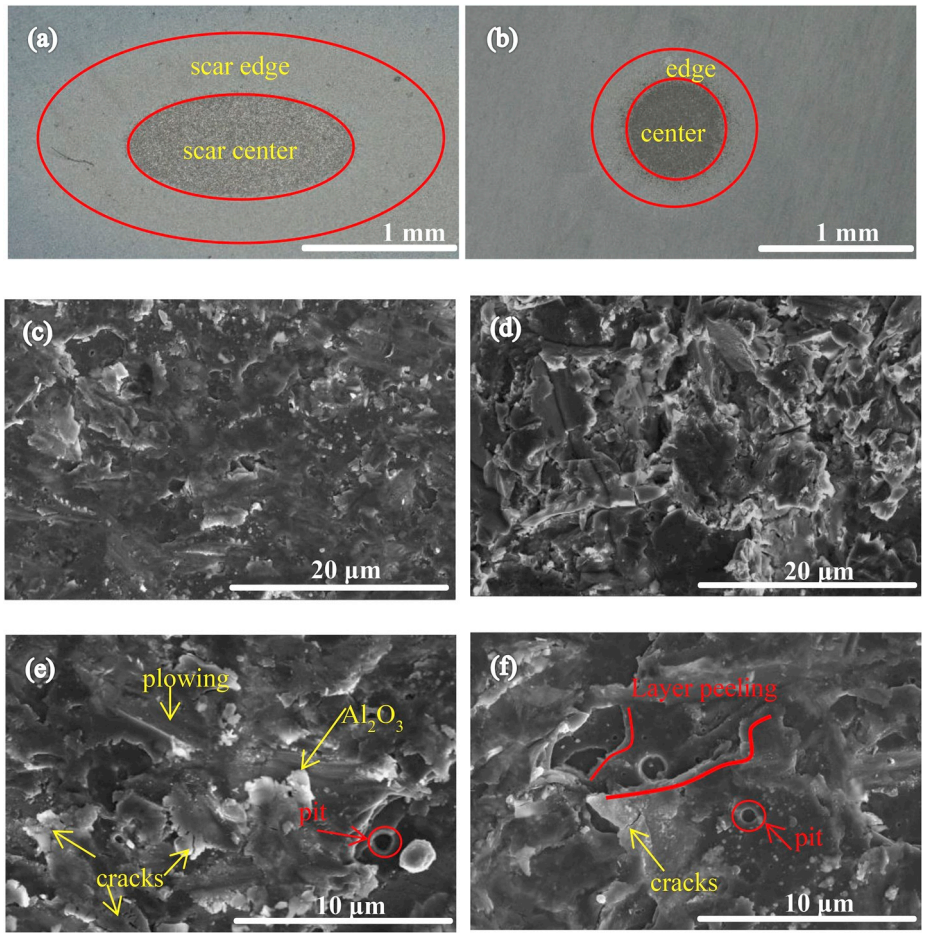

Fig. 10. Morphology of the CrAlNx/CrAlN coating after 30° and 90°eosion experiment (a) (b) Scar macroscopic appearance; (c) (d) Scar edge morphology; (e) (f) Scar center morphology.

is not difficult to find multiple interfaces (the lamellar and columnar interfaces, the thin and thick columnar interfaces). Due to the increase of the interlayer interface, the crack is easy to deflect and restrain at the interface, which prevents crack propagation [28]. In addition, when the metal-rich CrAlNx nano-layer is subjected to external stress, its monoclinal crystal density is low, and it is prone to deformation absorbing the energy of the main crack propagation, and weakening the crack propagation. Therefore, the high hardness and toughness, low residual stress and unique multilayer structure of the CrAlNx/CrAlN coating can maintain similar erosion resistance to hard coating during in the process of the small angle erosion. In addition, in the process of large angle erosion, due to its high toughness and structural characteristics, the generation and propagation of cracks are hindered. Finally, the solid particle erosion resistant of the CrAlNx/CrAlN multilayer coating is improved.

4. Conclusion

In this paper, the CrAlNx/CrAlN micro-nano multi-layer structure coating was designed and prepared. The microstructure, phase structure, mechanical properties and erosion properties of Cr-based coatings (CrN, CrAlN, CrAlNx/CrAlN) were studied, leading to the following conclusions:

1. The micro-structure of CrAlNx/CrAlN multilayer coating is consisted of lamellar, thin columnar structure and thick columnar structure. CrAlNx is composed of lamellar and fine columnar, and a large amount of nano-$Al_{13}Cr_2$ metal crystal phase is wrapped with a small amount of nano-AlN ceramic crystal phase.
2. The hardness of CrAlNx/CrAlN multilayer coating (24.7 ± 0.6 GPa) is similar to that of CrAlN monolayer coating (24.9 ± 0.3 GPa). However, multilayer coating have higher adhesion strength, fracture toughness, and minimum residual stress.
3. The average solid particle erosion rates of Cr-based coatings during 30° and 90° erosion: CrN 1.102 ± 0.033 μm/g, CrAlN 1.059 ± 0.032 μm/g, and CrAlNx/CrAlN 0.916 ± 0.029 μm/g. There are two reasons to explain why the multilayer coating is most resistant to erosion. On the one hand, the low residual stress and high adhesion strength make the coating difficult to peel. On the other hand, the unique multilayer structure improves the toughness and anti-crack propagation of the coating, and makes the coating have excellent solid particle erosion resistance.

Acknowledgements

This study is supported by Guangdong Science and Technology Program (NO. 2017A070701027, NO. 2014B070705007) and GDAS' Project of Science Technology Development (NO.2019GDASYL-0302012, NO. 2017GDASCX-0111 and NO. 2018 GDAS CX-0402). We gratefully acknowledge them for the financial support.

References

[1] A. Hamed, W.C. Tabakoff, R.V. Wenglarz, J. Propuls. Power 22 (2012) 350–360.
[2] Q. Yang, R. McKellar, Tribol. Int. 83 (2015) 12–20.
[3] F. Cai, X. Huang, Q. Yang, Wear 324 (2015) 27–35.

[4] E. Bousser, L. Martinu, J.E. Klemberg-Sapieha, Surf. Coat. Technol. 257 (2014) 165–181.
[5] M. Pepi, Richard Squillacioti, Lynne Pfledderer, J. Fail. Anal. Prev. 12 (2011) 96–108.
[6] Q. Yang, D.Y. Seo, L.R. Zhao, Surf. Coat. Technol. 188 (2004) 168–173.
[7] X.T. Zeng, T. Goto, L.R. Zhao, J. Vac. Sci. Technol. A Vac. Surf. Films 23 (2005) 288–292.
[8] M.W. Reedy, J. Timothy, K. John, Surf. Coat. Technol. 206 (2011) 464–472.
[9] S.S. Lin, K.S. Zhou, M.J. Dai, Vacuum 122 (2015) 179–186.
[10] A. Feuerstein, A. Kleyman, Surf. Coat. Technol. 204 (2009) 1092–1096.
[11] D.A. Colombo, D. Alejo Mandri, D. María Echeverría, Thin Solid Films 647 (2018). S0040609017309100.
[12] L.J. Yang, Z.H. Dang, X. An, Mater. Sci. Forum 789 (2014) 449–454.
[13] A. Feuerstein, A. Kleyman, Surf. Coat. Technol. 204 (2009) 1092–1096.
[14] P. Wieciński, J. Smolik, H. Garbacz, Vacuum 107 (2014) 277–283.
[15] M. Naveed, A. Obrosov, S. Weiß, Eur. Symp. Frict. 26 (2014) 366–373.
[16] J.L. Mo, M.H. Zhu, B. Lei, Wear 263 (2007) 1423–1429.
[17] N.J.M. Carvalho, E. Zoestbergen, B.J. Kooi, Thin Solid Films 429 (2003) 179–189.
[18] C.Q. Guo, Z.L. Pei, D. Fan, Mater. Des. 110 (2016) 858–864.
[19] B.R. Lawn, A.G. Evans, D.B. Marshall, J. Am. Ceram. Soc. 63 (1980) 9–10.
[20] ASTM G76-13, Standard Test Method for Conducting Erosion Tests by Solid Particle Impingement Using Gas Jets [S], 2013.
[21] L. Wang, G. Zhang, R.J.K. Wood, Surf. Coat. Technol. 204 (2010) 3517–3524.
[22] N.J.M. Carvalho, E. Zoestbergen, B.J. Kooi, Thin Solid Films 429 (2003) 179–189.
[23] M.H.G. Jacobs, R. Schmid-Fetzer, T. Markus, Intermetallics 16 (2008) 995–1005.
[24] F. Sanchette, T. Czerwiec, A. Billard, Surf. Coat. Technol. 96 (1997) 184–190.
[25] A. Dück, N. Gamer, W. Gesatzke, Surf. Coat. Technol. 142 (2001) 579–584.
[26] Q. Wang, F. Zhou, J. Yan, Surf. Coat. Technol. 285 (2016) 203–213.
[27] G.P. Tilly, Wear 23 (1973) 87–96.
[28] X. Xiao, D. Terentyev, Q. Chen, Int. J. Plast. 90 (2017) 212–230.